Neuron
Article

Oscillatory Synchronization in Large-Scale Cortical Networks Predicts Perception

Joerg F. Hipp,[1,*] Andreas K. Engel,[1] and Markus Siegel[1,2,3]
[1]Department of Neurophysiology and Pathophysiology, University Medical Center Hamburg-Eppendorf, 20246 Hamburg, Germany
[2]The Picower Institute for Learning and Memory, Massachusetts Institute of Technology, Cambridge, MA 02139, USA
[3]Centre for Integrative Neuroscience, University of Tübingen, 72076 Tübingen, Germany
*Correspondence: j.hipp@uke.de
DOI 10.1016/j.neuron.2010.12.027

SUMMARY

Normal brain function requires the dynamic interaction of functionally specialized but widely distributed cortical regions. Long-range synchronization of oscillatory signals has been suggested to mediate these interactions within large-scale cortical networks, but direct evidence is sparse. Here we show that oscillatory synchronization is organized in such large-scale networks. We implemented an analysis approach that allows for imaging synchronized cortical networks and applied this technique to EEG recordings in humans. We identified two networks: beta-band synchronization (~20 Hz) in a fronto-parieto-occipital network and gamma-band synchronization (~80 Hz) in a centro-temporal network. Strong perceptual correlates support their functional relevance: the strength of synchronization within these networks predicted the subjects' percept of an ambiguous audiovisual stimulus as well as the integration of auditory and visual information. Our results provide evidence that oscillatory neuronal synchronization mediates neuronal communication within frequency-specific, large-scale cortical networks.

INTRODUCTION

The brain is organized in a large number of functionally specialized but widely distributed cortical regions. Goal-directed behavior requires the flexible interaction of task-dependent subsets of these regions, but the neural mechanisms regulating these interactions remain poorly understood. Long-range oscillatory synchronization has been suggested to dynamically establish such task-dependent networks of cortical regions (Engel et al., 2001; Fries, 2005; Salinas and Sejnowski, 2001; Varela et al., 2001). Consequently, disturbances of such synchronized networks have been implicated in several brain disorders, such as schizophrenia, autism, and Parkinson's disease (Uhlhaas and Singer, 2006). However, in contrast to locally synchronized oscillatory activity, little is known about the global organization of long-range cortical synchronization. On the one hand, invasive recordings reveal task-specific synchronization between pairs of focal cortical sites (Buschman and Miller, 2007; Gregoriou et al., 2009; Maier et al., 2008; Pesaran et al., 2008; Roelfsema et al., 1997; Saalmann et al., 2007; von Stein et al., 2000), but require the preselection of recording sites and provide little information about the spatial extent and structure of synchronization patterns across the entire brain. On the other hand, electroencephalography (EEG) and magnetoencephalography (MEG) measure synchronized signals across widely distant extracranial sensors (Gross et al., 2004; Hummel and Gerloff, 2005; Rodriguez et al., 1999; Rose and Buchel, 2005), but it remains difficult to attribute these to neural synchronization at the cortical level. Hence, it has yet been difficult to demonstrate synchronization in functionally and anatomically specific large-scale cortical networks. The goal of this study was to test whether cortical synchronization is organized in such large-scale networks in the human brain. Furthermore, we aimed to characterize the spatial scale, structure, and spectral properties of such networks and sought to provide behavioral evidence for their functional relevance.

We developed a new analysis approach based on cluster permutation statistics that allows for effectively imaging synchronized networks across the entire human brain. We applied this approach to EEG recordings in human subjects reporting their alternating percept of an ambiguous audiovisual stimulus. The ambiguous stimulus had two major advantages: First, perceptual disambiguation activates widely distributed cortical regions, including frontal, parietal, and sensory areas (Leopold and Logothetis, 1999; Lumer et al., 1998; Sterzer et al., 2009), making it a prime candidate to identify large-scale synchronized cortical networks. Second, the alternating percepts in face of constant stimulation provided a critical test for the functional relevance of such synchronized networks: We investigated whether intrinsic fluctuations of synchrony predicted the subjects' percept.

RESULTS

Behavior and Local Cortical Population Activity

On each trial, subjects (n = 24) were presented with an identical ambiguous audiovisual stimulus: two bars approached, briefly overlapped while a click sound was played, and moved apart from each other (Figure 1). As previously reported (Bushara et al., 2003; Sekuler et al., 1997), perception of this stimulus

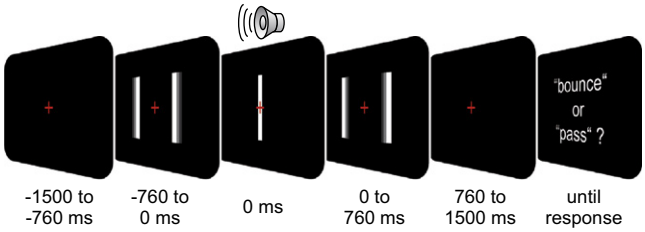

Figure 1. Behavioral Task

On each trial, subjects fixated a central cross while two moving bars approached each other, overlapped, and diverged again (total duration, 1.52 s). At the moment of overlap (t = 0 s), a click-sound was played (duration, 0.02 s). The stimulus was either perceived as two bars passing each other (pass) or bouncing off each other (bounce). Subjects reported their percept via button-press (left/right thumb) after fixation cross offset (0.76 s after stimulus offset; counterbalanced percept-response mapping across subjects).

spontaneously alternated between two distinct alternatives. For one set of trials ("bounce" trials; 52.2%), the two bars were perceived as bouncing off each other. For the other set of trials ("pass" trials; 47.8%), the two bars were perceived as passing one another. After each stimulus presentation and a brief delay, subjects reported their percept by button press.

Stimulus presentation modulated local cortical population activity in a frequency-specific fashion (Figure 2). We employed distributed source-analysis ("beamforming") to estimate local neural population activity throughout the cortex as a function of time and frequency (see Experimental Procedures). We then quantified the change in neural activity during stimulation relative to the prestimulus baseline. In accordance with human MEG (Donner et al., 2007; Gruber et al., 1999; Hall et al., 2005; Jensen et al., 2007; Siegel et al., 2007, 2008; Tallon-Baudry et al., 1996; Wyart and Tallon-Baudry, 2008) and invasive animal experiments (Gray and Singer, 1989; Gregoriou et al., 2009; Henrie and Shapley, 2005; Siegel and König, 2003), across most of visual cortex, stimulation induced a tonic increase of neural activity in the high gamma band (64–128 Hz), while activity in the theta (5–8 Hz), alpha (8–16 Hz), and beta (16–32 Hz) bands was reduced. Recovering this well-known spectral signature of visual stimulation demonstrates that EEG in combination with source-analysis allows for reconstructing cortical population signals across the entire investigated frequency range. In addition to the response in visual cortex, we found a tonic increase in the alpha band (8–16 Hz) in bilateral frontal regions consistent with the frontal eye fields (FEF).

Identifying Networks of Cortico-Cortical Synchronization

We proceeded by analyzing whether local population activity was synchronized between distant cortical regions. Our analysis approach rested on two fundaments.

First, we addressed important methodological problems limiting the interpretation of measures of neural interaction derived from EEG or MEG. A key problem is to resolve whether synchrony measured between distant locations reflects truly synchronized neural activities or merely a single neural source picked up at different locations. To account for this problem,

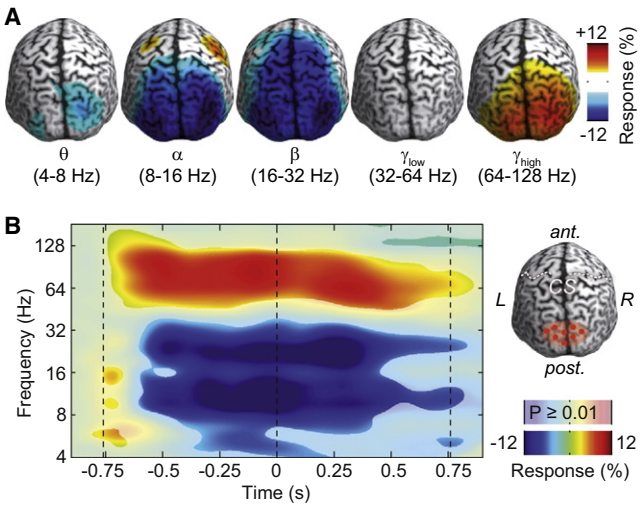

Figure 2. Local Neural Population Activity

(A) Power response during stimulation (−0.25 to 0.25 s) relative to the prestimulus baseline in the theta (4–8 Hz), alpha (8–16 Hz), beta (16–32 Hz), low gamma (32–64 Hz), and high gamma (64–128 Hz) bands. Responses are visualized on the standard MNI-brain viewed from the top back (see Experimental Procedures and Figure S1).

(B) Power response relative to prestimulus baseline resolved in time and frequency for an occipito-parietal region of interest. The region of interest is visualized on the right; CS: central sulcus.

we analyzed synchronization at the source level, which critically improves spatial specificity by transforming the unspecific sensor signals into localized source estimates (Kujala et al., 2008; Schoffelen and Gross, 2009; Siegel et al., 2008). Furthermore, we investigated functional modulations rather than absolute levels of synchronization. This subtracted out the spatial pattern of synchronization induced by the limited spatial resolution that is common to any two conditions compared. Another crucial but often ignored problem is that interaction measures of neural population signals depend on the relative weighting of different signal components (Nunez and Srinivasan, 2006). Specifically, they depend on the weighting of the neural signal of interest relative to noise and neural signals that are not of interest. Thus, even if the true interaction between the signal components remains constant, changes in the components' amplitudes may alter their relative weighting and cause a change in the measured interaction between the population signals. We addressed this problem by comparing changes in synchrony to concurrent changes in signal amplitude (see Supplemental Experimental Procedures available online).

Second, we devised a new analysis approach that allows for identifying networks of synchronized cortical regions (Figure S2 available online). In brief, we employed permutation statistics to identify cortical networks as continuous clusters in a high-dimensional interaction space (see Experimental Procedures). This allowed for directly identifying networks across a full pairwise cortico-cortical space. We applied this approach to source-level coherence estimated from EEG (Gross et al., 2001), which quantifies the frequency-specific phase consistency between regions. This allowed us to effectively image

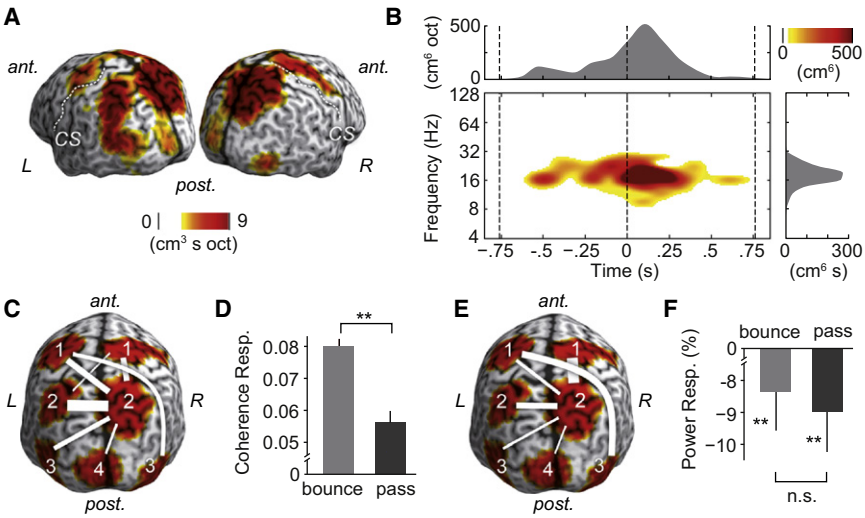

Figure 3. Perception-Related Beta-Synchrony Network

(A) Spatial localization of cortical regions engaged in the network. For each cortical location, the color shows for how long, across which frequency-range, and to how many other locations coherence was increased for bounce and pass trials relative to baseline (CS: central sulcus).

(B) Bottom left: Spectro-temporal coherence profile of the network that displays between how many locations coherence was increased at a given time and frequency. Top and right: Corresponding temporal and spectral coherence profiles. The spectral profile ranged from 15–23 Hz (full width at half maximum, FWHM).

(C) Coherence structure between the seven clusters forming the beta-network (stimulation versus baseline). Line-width represents relative coherence strength. 1, frontal cortex; 2, posterior parietal cortex; 3, lateral occipitotemporal cortex; 4, medial occipital cortex.

(D) Coherence response relative to prestimulus baseline for bounce and pass percepts within the beta-network (mean ± SEM).

(E) Structure of difference in coherence between bounce and pass percepts. Line-width represents relative coherence strength.

(F) Power response relative to prestimulus baseline for bounce and pass percepts within the beta-network (mean ± SEM).

synchronized cortical networks across space, time, and frequency. Importantly, no a priori assumptions had to be made about the time and frequency of synchronization or about the number, size, location, and spatial structure of the synchronized networks.

Beta-Synchrony Network

We first applied this network-identification approach to contrast cortico-cortical coherence between the stimulation and baseline intervals. This revealed a widespread but highly structured cortical network (Figures 3A and 3B, permutation-test, $p = 0.0245$) that showed enhanced beta-band coherence (15–23 Hz) during stimulation. The network consisted of a largely symmetric pattern of cortical regions spanning extrastriate visual areas implicated in the processing of visual motion as well as higher order association areas. Bilaterally, it included frontal regions consistent with the FEF, posterior parietal cortices along the intraparietal sulcus (IPS), lateral occipitotemporal cortices consistent with the middle temporal area (MT+), and medially extrastriate visual cortex near the transversal occipital sulcus (see Table S1 available online). Beta-band coherence in this network was enhanced for about 1 s around the time of bar overlap (Figure 3B). We further quantified the detailed pattern of synchronization between the different nodes within the network (Figure 3C). This revealed a hublike structure in which the right posterior parietal cortex synchronized most prominently with other nodes of the network. Thus, in contrast to the widespread stimulus-related decrease in local beta-band activity (compare Figure 2B), long-range beta-synchrony was enhanced in a highly structured network during stimulus presentation.

If beta-band synchronization within this network was functionally relevant for processing of the sensory stimulus, intrinsic fluctuations of synchrony may predict the subjects' alternating perception of the constant physical stimulus. Indeed, we found that beta-synchrony was not only enhanced during stimulus processing but also predicted the subjects' percept of the stimulus. We compared coherence within the identified network for trials in which the subjects perceived the stimulus as "bouncing" or "passing." This yielded a highly significant difference (Figure 3D, permutation-test, $p < 0.0001$) with enhanced beta-coherence for bounce trials. Receiver operating characteristic (ROC) analysis revealed that, even on a single-trial level, the strength of beta-coherence significantly predicted the subjects' percept (permutation-test, $p < 0.0001$). In other words, when large-scale beta-band synchronization was enhanced between frontal, parietal, and extrastriate areas, subjects were more likely to perceive the same sensory stimulus as bouncing rather than passing. Although this percept-predictive difference in synchronization overall had a network structure similar to the stimulus-related increase in synchrony, we found the strongest perception-related effects for synchronization with frontal regions (Figure 3E).

In principle, differences in neural activity between bounce and pass trials may either reflect neural processes directly causing the subjects' percepts or, alternatively, may reflect only secondary processes ensuing from the alternating percept. The time course of neural activity relative to the perceptual ambiguity provides critical evidence to resolve this question. We thus exploited the temporal resolution of EEG and tested whether the difference in coherence temporally preceded the time when the stimulus became ambiguous ($t = 0$ s). Indeed, we found that already before the time of bar overlap (time < -0.125 s; accounting for the size of the analysis window) coherence significantly predicted the subjects' percepts (ROC analysis, permutation-test, $p = 0.0002$). This provides strong evidence that, rather than merely being a consequence of the different percepts, fluctuations of large-scale beta-synchrony in fact determined the perceptual interpretation of the stimulus.

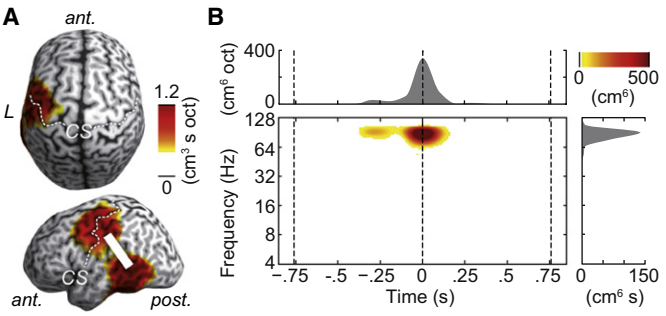

Figure 4. Perception-Related Gamma-Synchrony Network

(A) Spatial localization of cortical regions engaged in the network. For each cortical location, the color shows for how long, across which frequency-range, and to how many other locations coherence was increased for bounce relative to pass trials (CS: central sulcus).

(B) Bottom left: Spectro-temporal coherence profile of the network that displays between how many locations coherence was increased at a given time and frequency. Top and right: Corresponding temporal and spectral coherence profiles. The spectral profile ranged from 74 to 97 Hz (FWHM).

(C) Coherence response relative to prestimulus baseline for bounce and pass percepts within the gamma-network (mean ± SEM).

(D) Power response relative to prestimulus baseline for bounce and pass percepts within the gamma-network (mean ± SEM).

Modulations of neural synchronization in the beta-network could not simply be explained by changes in signal power. We first compared power within the identified beta-synchrony network between bounce and pass trials (Figure 3F). There was no significant difference (permutation-test, $p = 0.34$) suggesting that the difference in coherence between bounce and pass percepts reflected a true change in oscillatory synchronization rather than a change in the weighting of the beta-activity of interest relative to other signal components. Second, the stimulus-related increase in beta coherence was accompanied by a significant decrease in signal power (Figures 3D and 3F), raising the question of whether the coherence increase merely reflected this change in signal power. The different topographies and time courses of the coherence and power modulations argue against this explanation. Although coherence was modulated in a distinct network with several local nodes (Figure 3), power changes in the beta band were spatially more widespread and also of longer duration (Figure 2). Furthermore, if the stimulus-related decrease in power accounted for the increase in coherence, this negative correlation should also hold on the single-trial level (under the assumption that the single-trial fluctuation in beta-power was driven by the same signal or noise component as the difference between stimulus and baseline intervals). To the contrary, beta power and coherence were positively correlated on the single-trial level (correlation of single-trial coherence pseudovalues and single-trial power; Pearson's correlation coefficients, $r = 0.065$; permutation-test, $p = 0.0014$). These two lines of evidence also suggest that the stimulus-related increase in beta-coherence was not driven by a change in signal power. In contrast, we identified another network with increased coherence during stimulation that may have well been confounded by changes in signal power (Figure S3). The spectro-temporal profile and spatial localization of the coherence-modulation in this network closely resembled the stimulus-driven increase in gamma power. Taken together, these results demonstrate large-scale beta-synchronization in a distinctive network of frontal, parietal, and extrastriate visual areas during stimulus processing that predicted the subjects' percept on the single-trial level.

Gamma-Synchrony Network

We identified the above network on the basis of changes in synchrony relative to baseline. However, synchronization could also differ between bounce and pass trials while altogether not changing relative to baseline (independent contrasts). We thus directly contrasted trials with bounce and pass percepts using our network-identification approach. This revealed a left hemispheric network consisting of central and temporal regions that showed significantly stronger high gamma-band coherence (74–97 Hz) for bounce than for pass trials (Figures 4A and 4B; permutation-test, $p = 0.0071$). This perception related gamma-band synchronization started before and peaked around the time of bar overlap (Figure 4B). The difference in coherence was caused by an increase during bounce trials (Figure 4C, permutation-test, $p < 0.0001$) and a decrease during pass trials (Figure 4C, permutation-test, $p < 0.0001$) relative to the average prestimulus baseline. We confirmed the left lateralization of the network: Coherence did not differ between bounce and pass trials at the corresponding locations in the right hemisphere (permutation-test, $p = 0.67$). Contrasting trials with a left and right hand responses, we ruled out that the network reflects preparation of the specific motor response (permutation-test, $p = 0.76$). As for the beta-network, we found that changes in coherence were not accompanied by potentially confounding changes in signal power. There was no difference in gamma-power between bounce and pass trials (Figure 4D, permutation-test, $p = 0.50$).

In addition to the subjects' percept, gamma-band synchronization in the above network was directly linked to the cross-modal integration of auditory and visual information. For the present stimulus, this cross-modal integration is reflected by the fact that the auditory stimulus biases the visual percept toward the bounce interpretation. In fact, on bounce trials, the click-sound is perceived as being caused by the collision of the two bars. In accordance with previous reports (Bushara et al., 2003; Sekuler et al., 1997), we psychophysically confirmed this auditory bias on perception. The rate of bounce percepts was significantly higher for the audiovisual stimulus compared to a unimodal visual control stimulus (Figure 5A, bounce audiovisual, 52.2%; bounce visual control, 32.5%; permutation-test, $p < 0.0001$). For each subject, we quantified this cross-modal bias as the difference in probability of observing the bounce percept between the audiovisual stimulus and the unimodal visual control.

The interindividual difference in this cross-modal bias was reflected in the strength of synchronization within the gamma-network. Across subjects, we found a highly significant negative correlation between the cross-modal bias and the difference

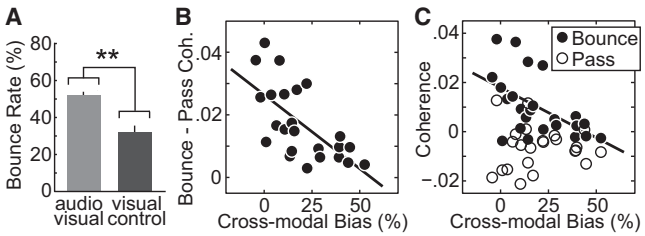

Figure 5. Synchronization in the Gamma-Network Reflects Cross-Modal Bias

(A) Behavioral data. When the audiovisual stimulus was presented, subjects more often perceived the bars as bouncing compared to the visual-only control stimulus (mean ± SEM).

(B) Correlation between the subjects' percept-specific coherence in the gamma network (bounce-pass coherence) and the individual cross-modal bias.

(C) Correlation of coherence on bounce and pass trials relative to the average prestimulus baseline with the subjects' cross-modal bias.

between gamma-band coherence for bounce and pass trials (Figure 5B; Pearson correlation coefficient, $r = -0.66$, $p = 0.0004$). This correlation was specifically attributable to coherence on bounce trials (Figure 5C; bounce, $r = -0.54$ and $p = 0.0054$; pass, $r = 0.15$ and $p = 0.48$). Interestingly, the difference in synchronization was strongest for subjects without cross-modal bias and vanished for subjects with a strong bias. In other words, enhanced synchronization predicted the cross-modally integrated bounce percept specifically for those subjects who showed a weaker cross-modal bias, as if more synchronization would be required to support the bounce percept for these subjects. Despite not revealing the detailed underlying mechanism, this correlation established a direct link between long-range oscillatory synchronization and cross-modal processing on the population level.

Again, the effect did not simply reflect changes in signal power, which did not show a significant correlation with the cross-modal bias (bounce versus pass, $r = 0.094$ and $p = 0.66$; bounce, $r = -0.16$ and $p = 0.45$). The correlation between coherence and cross-modal bias was specific to the gamma-band network. The beta-network did not show a corresponding effect ($r = 0.22$; $p = 0.31$). Furthermore, the correlation of neural synchrony with the cross-modal bias could not be explained by a correlation of synchrony with the general probability to perceive the stimulus as bouncing. There was no significant correlation between the perceptual difference in coherence and the absolute bounce rate ($r = -0.16$; $p = 0.45$). Importantly, temporal precedence again suggested that, rather than being a consequence, large-scale synchrony indeed determined the cross-modal integration of sensory information: The difference in coherence in the gamma-network directly before the presentation of the sound (time < -0.125; accounting for the size of the analysis window) significantly predicted the subjects' cross-modal bias of the percept by the upcoming auditory stimulus ($r = -0.53$; $p = 0.0073$).

Control Analyses

The perception-related coherence within the above reported networks was robust across several control analyses. First, the EEG can be contaminated by microsaccade artifacts (Yuval-Greenberg et al., 2008). Thus, we repeated all central analyses after EOG-based detection and removal of EEG data contaminated by microsaccade artifacts (Keren et al., 2010). All these control analyses confirmed the reported results. For the beta-network, the increase in coherence during stimulation and the difference between bounce and pass trials were not affected by microsaccade artifacts (permutation-test, both $p < 0.0001$). Similarly, for the gamma-network, the difference in coherence between bounce and pass trials (permutation-test, $p < 0.0001$) and the correlation with the cross-modal bias (correlation coefficient, $r = -0.53$; $p = 0.007$) were unaffected.

Second, coherence estimates can be affected by changes in amplitude correlation. Thus, we repeated all central analyses based on the "phase-locking value," which quantifies phase-consistency independent of amplitude correlations (Lachaux et al., 1999). Again, this confirmed all reported results. For the beta network, the phase-locking value increased during stimulation and was greater for bounce as compared to pass trials (permutation-test, both $p < 0.0001$). For the gamma network, the phase-locking value was larger for bounce than for pass trials (permutation-test, $p < 0.0001$) and this difference was significantly correlated with the cross-modal bias across subjects (correlation coefficient, $r = -0.66$; $p < 0.0005$).

Perceptual Correlates in Local Population Activity

Compared to the prominent perception related effects of long-range oscillatory synchronization, we found only weak effects for local population activity. We modified our network-identification approach to image perception–related changes in local signal power (see Experimental Procedures). This did not reveal any significant differences between bounce and pass trials. Only using a "less conservative" statistic (fixed-effects analysis), we found a late power difference in the low gamma-band that emerged 300 ms after bar overlap (peak at 600 ms) and was localized in left frontal cortex, compatible with the FEF (27–52 Hz; permutation-test, $p = 0.02$) (Figure S4). Thus, in contrast to long-range synchronization, which predicted perception before the stimulus became ambiguous, changes in power rather seemed to reflect a consequence of the establishment of the different percepts.

DISCUSSION

In summary, our results demonstrate highly structured large-scale cortical networks of oscillatory synchronization: up to seven anatomically confined cortical areas synchronized their activities across several centimeters and multiple processing stages along the sensorimotor pathways. Synchronization within these networks was temporally well localized to the cognitive event of interest and was linked to specific frequency ranges that differed across multiple octaves between networks (beta and gamma).

Although much progress has been made studying neural population activity in individual cortical areas, it remains difficult to characterize large-scale neural interactions across the entire brain. This is largely due to methodological problems. On the one hand, it is difficult to simultaneously record from multiple

brain regions in invasive experiments. On the other hand, although EEG and MEG sample neural activity from a large part of the brain, estimating cortical interaction on the basis of these extracranial signals remains difficult. A further important obstacle is the lack of tools to efficiently analyze cortico-cortical interactions in a high-dimensional space with the ensuing substantial multiple-comparison problem. Our cluster-permutation–based approach may provide a valuable new tool to address these problems and to identify large-scale networks of interacting sources. In particular, it goes beyond imaging neural activity across a singular cortical space and provides a framework to characterize interactions in a full pairwise cortico-cortical space. In principle, the approach is not limited to the study of synchrony, as demonstrated here, but may be applied to any bivariate parameter defined across the brain. Furthermore, the approach can be applied to a broad spectrum of experimental designs, including simple condition differences as well as complex parametric models. Moreover, no a priori assumptions need to be made about the structure of cortical networks. The method is robust to oversampling of the pairwise interaction space. This allows for directly imaging the extent of networks in space, time, and frequency. This approach well complements recent applications of graph-theoretical measures that provide powerful tools to quantify the global structural properties of large-scale connectivity (Bressler and Menon, 2010; Hagmann et al., 2008; Palva et al., 2010).

Our results provide strong evidence for the functional relevance of synchronization within the identified large-scale cortical networks. For identical sensory stimulation, the subjects' percept was predicted by intrinsic fluctuations of long-range synchronization directly preceding the sensory ambiguity. The first network, synchronizing in the beta-band (Figure 3), consisted of frontal (FEF) and parietal (posterior IPS) regions that have been implicated in multistable perception (Leopold and Logothetis, 1999; Lumer et al., 1998; Sterzer et al., 2009) and the control of selective attention (Barcelo et al., 2000; Corbetta and Shulman, 2002; Kastner and Ungerleider, 2000; Moore et al., 2003; Posner and Dehaene, 1994; Serences and Yantis, 2006). Furthermore, the network included early sensory processing stages selective for the ambiguous feature at hand (here: visual motion, MT+) (Tootell et al., 1995). Thus, fluctuations of beta-synchrony between these stages may reflect fluctuations of visual attention that modulate the perceptual organization of the stimulus, with strong interactions favoring the bounce percept. Our results extend previous findings that have implicated beta-band activity across frontal and parietal regions in visual attention, decision making, and sensorimotor integration (Buschman and Miller, 2007; Donner et al., 2007; Gross et al., 2004; Kopell et al., 2000; Pesaran et al., 2008; Roelfsema et al., 1997). We propose that beta-band synchronization may serve as a general mechanism mediating large-scale interactions across a network of frontal, parietal, and extrastriate visual areas.

The second network synchronizing in the gamma-band (Figures 4 and 5) included central areas consistent with sensorimotor and premotor regions, as well as temporal areas. Both regions have been implicated in multisensory processing. Premotor regions are responsive to auditory, visual, and somatosensory stimuli (Fogassi et al., 1996; Graziano et al., 1994, 1999; Lemus et al., 2009), and temporal regions are involved in the cross-modal integration of audiovisual stimuli (Barraclough et al., 2005; Bushara et al., 2003; Dahl et al., 2009; Maier et al., 2008; Noesselt et al., 2007; Schneider et al., 2008). Consistent with this evidence, fluctuations of synchrony within the gamma network did not only reflect the subjects' percept of the ambiguous stimulus but also predicted interindividual differences in the cross-modal integration of auditory and visual information. Enhanced synchronization was specifically associated with the cross-modally more integrated bounce percept. These results accord well with recent accounts of cross-modal processing that emphasize the role of recurrent interactions between processing streams traditionally considered as unimodal as well as between early sensory and higher-order multimodal processing stages (Driver and Noesselt, 2008; Driver and Spence, 2000; Ghazanfar and Schroeder, 2006; Kayser et al., 2008; Lakatos et al., 2007; Lewis and Noppeney, 2010; Meredith et al., 2009; Stein and Meredith, 1993). Our results provide evidence that long-range synchronization between cortical regions may mediate such interactions and thus play an important role for the cross-modal integration of sensory information (Maier et al., 2008; Senkowski et al., 2008).

Our results reveal a surprising dissociation between local oscillatory activity and long-range synchronization. The enhanced long-range beta-synchrony during stimulus processing was contrasted by a profound and widespread suppression of local beta-band activity. Also, the perceptual effects of long-range synchrony were not accompanied by corresponding modulations in local population activity. This indicates that the frequency-specific synchronization between regions can be dissociated from their local oscillatory activity. Distant cortical sites may synchronize their activity in a specific frequency range without corresponding changes of local population activity.

Our results show that large-scale cortical synchronization is expressed in widespread but highly structured networks and it is tightly linked to the perceptual organization of sensory information. This adds to a growing body of evidence showing that large-scale cortical synchronization plays an important role in various cognitive functions including selective attention (Buschman and Miller, 2007; Gregoriou et al., 2009; Saalmann et al., 2007; Siegel et al., 2008), cross-modal integration (Maier et al., 2008), decision making (Pesaran et al., 2008), sensorimotor integration (Bressler et al., 1993; Roelfsema et al., 1997), and working memory (Palva et al., 2010).

Membrane-potential oscillations establish periodic windows of enhanced excitability (Haider and McCormick, 2009; Lakatos et al., 2005). Thus, oscillatory synchronization between presynaptic spikes and such postsynaptic fluctuations may modulate the efficiency of information transmission (Fries, 2005; Womelsdorf et al., 2007). The perceptual correlates of long-range synchronization demonstrated here provide evidence that such activity may indeed mediate the information flow within large-scale cortical networks. The disturbances of such large-scale patterns of synchronization may play an important role in several brain disorders (Uhlhaas and Singer, 2006). The cluster-based network identification approach provides a promising new technique to characterize such synchronized networks

and to investigate their role in normal and impaired human brain function.

EXPERIMENTAL PROCEDURES

Here we provide a brief account of the applied methods. Please see the Supplemental Experimental Procedures online for full details.

Participants, Stimuli, and Task

EEG recordings were performed in 24 subjects (12 female; mean age, 25 years; all right handed). All participants had normal hearing, normal or corrected-to-normal vision, and had no history of neurological or psychiatric illness. Subjects were presented with two types of stimulation: an audiovisual stimulus (500 trials) and a subsequent visual-only control stimulus (100 trials). Visual stimulation was identical as described in Figure 1 (size of bars, 5° × 0.125° visual angle; starting position at 3.8° eccentricity; velocity of 5°/s), but on audiovisual trials a click-sound (duration, 20 ms; volume, 60 dB SPL) was played at the moment of bar overlap via a central loudspeaker. Subjects reported their percept of the ambiguous stimulation via button-press (left and right thumb) after fixation-cross offset. The percept-response mapping was counterbalanced across subjects. The study was conducted in accordance with the Declaration of Helsinki and informed consent was obtained from all participants prior to the recordings.

Data Acquisition and Preprocessing

We recorded the continuous EEG from 126 scalp sites referenced against the nose tip. Electrode impedances were kept below 20 kΩ. For artifact cleaning, we split the data set into two frequency bands (low frequencies, 4–34 Hz; high frequencies, 16-250 Hz). While eye movements and heartbeats cause low frequency artifact, muscle activity induces high-frequency artifact of the EEG signal. Separating these two artifact regimes allowed for more efficient artifact detection and removal. After filtering, the data were cut into trials of 2.5 s duration (−1.25 to 1.25 s). Trials with eye movements, eye blinks, or strong muscle activity were identified by visual inspection and rejected for both frequency bands. To reduce remaining artifacts (e.g., small eye movements, muscle twitches, and cardiac artifacts), we applied independent component analysis (Hyvarinen, 1999; Jung et al., 2000), separately for high and low frequencies, and rejected components that reflected signal artifacts. The selection of artifact components was based on careful inspection of their topography, power spectrum, and relation to the temporal structure of the experiment (mean ± SD number of rejected components: high frequency, 38 ± 10.5; low frequency, 14.5 ± 8.2). Preprocessing resulted in 179 ± 38.3 (mean ± SD) bounce trials and 167 ± 39.6 (mean ± SD) pass trials per subject. For all analyses, we recombined the data of the low- and high-frequency bands after the transformation to the frequency domain. To control for potential microsaccade artifacts (Yuval-Greenberg et al., 2008), we repeated all tests for coherence modulations within the identified cortical networks (see below) after removing data that were confounded by microsaccades (EOG based detection; Keren et al., 2010).

Spectral Analysis

All spectral estimates were performed using the multitaper method based on discrete prolate spheroidal (slepian) sequences (Mitra and Pesaran, 1999; Thomson, 1982). The mean frequencies and bandwidth of experimentally observed brain oscillations typically follow a linear progression on a logarithmic scale (Buzsaki and Draguhn, 2004). Accordingly, we computed spectral estimates across 23 logarithmically scaled frequencies from 4 to 181 Hz (0.25 octave steps) and across 23 points in time from −1.1 to 1.1 s (0.1 s steps). We adjusted the temporal and spectral smoothing using the multitaper method to match ~250 ms and 3/4 octave, respectively. For frequencies ≥16 Hz, we used temporal windows of 250 ms and adjusted the number of slepian tapers to approximate a spectral smoothing of 3/4 octave. For frequencies <16 Hz, we adjusted the time window to yield a frequency smoothing of 3/4 octaves with a single taper. We characterized power and coherence response relative to the prestimulus baseline using the bin at t = −0.9 s as a baseline for frequencies >5 Hz. For the lowest frequencies of 4 Hz and 4.8 Hz, we used baseline bins at t = −0.7 and t = −0.8 s, respectively, to keep the large temporal windows for the frequency transform within the range of the preprocessed data. For frequencies above and below 25 Hz, we computed the frequency transform on the basis of the high- and low-frequency data, respectively. We then continued the analysis across the combined spectral data. The employed time frequency transformation ensured a homogenous sampling and smoothing in time and frequency, as required for subsequent clustering within this space (see below).

Source Analysis

We used adaptive linear spatial filtering ("beamforming"' Gross et al., 2001; Van Veen et al., 1997) to estimate the spectral amplitude and phase of neural population signals at the cortical source level. In short, for each time, frequency, and source location, three orthogonal filters (one for each spatial dimension) were computed that pass activity from the location of interest with unit gain, while maximally suppressing activity from all other sources. We linearly combined the three filters to a single filter in the direction of maximal variance. To derive the complex source estimates, we multiplied the complex frequency domain data with the real-valued filter. The adaptive filter could induce spurious effects when comparing conditions. To avoid this, each trial was passed through a filter that was derived from the same amount of data from both conditions. We estimated cortical activity at 400 source locations that homogeneously covered the space below the electrodes at approximately 1 cm beneath the skull and a spacing of 1 cm. This coverage is well adapted to the spatial resolution of EEG and samples sources relatively close to the sensors with a high signal-to-noise ratio. To derive the leadfields (physical forward model), we first constructed a boundary element head model from the segmented MNI template brain. We then averaged the electrode positions measured in seven subjects and mapped these average positions to MNI space. Finally, we transformed the head model and electrode positions into the subjects' individual head space based on individual T1-weighted structural magnetic resonance images (MRI) and derived the leadfield in the subjects' space. We used the generic MNI-based leadfield for four of 24 subjects for whom no MRI was available.

It should be noted that high source correlations can reduce source amplitudes estimated with beamforming due to source cancellation (Van Veen et al., 1997). This may, in turn, affect the magnitude of cortico-cortical coherence estimates. However, in the range of physiological source-correlations (Leopold et al., 2003), this does not prevent the identification of cortico-cortical coherence using beamforming (Gross et al., 2001; Kujala et al., 2008). Moreover, although source-cancelation may affect the magnitude of, and reduce the sensitivity to detect coherence, it may not lead to false positive results.

Coherence Analysis

We estimated "coherence" to quantify the frequency-dependent synchronization between pairs of signals. Coherence quantifies the consistency of the phase and amplitude relation between two signals across repetitions. To estimate coherence on the single-trial level, we computed single-trial coherence pseudovalues (STCP, Jarvis and Mitra, 2001; Womelsdorf et al., 2006). Coherence is positively biased with decreasing number of independent spectral estimates (degrees of freedom). Thus, for all comparisons, we stratified the sample size and used the same number of trials for both conditions. The distribution of coherence values is highly non-Gaussian, violating the assumption of many parametrical tests. Thus, before statistical testing, we applied a nonlinear transform (Jarvis and Mitra, 2001) that renders the distribution approximately Gaussian. To ensure that changes in coherence reflected changes in phase consistency, rather than changes in signal amplitude, we retested all central results based on the phase-locking value (Lachaux et al., 1999).

Identification of Synchronized Networks

The general idea of our network identification approach can be summarized as follows: An interaction between two cortical areas can be formalized as a point in a six-dimensional space, consisting of the three-dimensional spatial coordinates of both areas. This interaction can extend into additional dimensions (e.g., time and frequency) increasing the total dimensionality of the connection space (e.g., to eight dimensions). In our approach, identifying significant interaction networks is equivalent to identifying continuous clusters within this

high-dimensional space. In other words, a network is a cluster of interactions that extends continuously across pairwise space and possible additional dimensions (e.g., time and frequency). To identify such clusters, we threshold the modulation of a neuronal interaction measure for each bin across the entire connection space, apply spatial filtering to the thresholded data, identify continuous clusters above the threshold, and evaluate their significance using a random permutation statistics that accounts for multiple comparisons across the interaction space. Cortical networks with many nodes may result in the identification of several spatially overlapping clusters. Such fragmentation depends in particular on the signal-to-noise ratio of the interaction measure at hand and the strength of applied neighborhood filtering. Thus, assembling overlapping clusters into larger clusters may optionally follow the cluster-identification step. For the present data, no overlapping clusters were identified.

We applied the network-identification approach to source-level coherence estimated from scalp-EEG as a function of time and frequency: In a first step, we computed coherence between all pairs of sources (400 × 400), at each point in time (n = 17; −0.8 to 0.8 in steps of 0.1) and frequency (n = 21; 4 to 128 Hz in steps of 0.25 octaves), and for each subject and condition. This results in an eight-dimensional space of connections (time × frequency × 3D space × 3D space). A single voxel in this space has a "volume" of 0.025 cm^6 × s × oct (1 cm^3 × 1 cm^3 × 0.1 s × 0.25 octave). To compare coherence between conditions (bounce versus pass; stimulation versus baseline), we computed a t-statistic of the difference in z-transformed coherence between conditions across subjects (random effects statistic). We thresholded the t-statistic at p = 0.01, resulting in a binary matrix with 0 for "smaller than threshold" ("no connection") and 1 for "larger than threshold" ("connection"). We then performed a neighborhood filtering (filter parameter, 0.5) by removing each connection that has a fraction of less than 0.5 directly neighboring connections (i.e., locations that differ by one unit in a single dimension, such as the same position and frequency but one time step difference). The neighborhood filtering results in a low-pass filtering of the connection-space and removes spurious bridges between connection clusters. We identified clusters in the eight-dimensional connection space as groups of connections that are linked through direct neighborhood relations (neighboring voxels with 1). Such a cluster corresponds to a network of cortical regions with different synchronization between conditions that is continuous across time, frequency, and pairwise space. For each cluster, we defined its size as the integral of the t-scores (condition difference) across the volume of the cluster and tested its statistical significance using a permutation statistic. We repeated the cluster identification 10^4 times (starting with the t-statistic between conditions) with shuffled condition labels to create an empirical distribution of cluster sizes under the null-hypothesis of no difference between conditions. The null-distribution was constructed from the largest clusters (two-tailed) of each resample therefore accounting for multiple comparisons (Nichols and Holmes, 2002). To optimize statistical sensitivity, we applied a Holm-correction (Holm, 1979): If a significant cluster was found, we removed the most significant cluster from the eight-dimensional space and repeated the analysis until no significant cluster remained.

To identify functional modulations of local rhythmic population activity, we modified our analysis approach to test for significant changes in source-level power: We compared signal power at all source locations (400) and at each point in time and frequency (17 × 21) between conditions (stimulation versus baseline; bounce versus pass). We then proceeded as for source-level coherence, but without neighborhood filtering. This resulted in clusters that represent significant changes in signal power across space, time, and frequency. We compared conditions using both random effects (across subjects) and fixed effects (pooled across subjects) statistics.

Illustration of Identified Networks

To visualize the identified networks we separately projected them onto different subspaces. To display the spatial extent (Figures 3A and 4A), we computed for each location the integral of the corresponding cluster in the connection space over time, frequency, and target locations. This integral was then displayed on the brain surface. This visualization reveals the spatial extent of the network independent of its intrinsic synchronization structure and location in time and frequency. Complementary to the spatial projection, we visualized the spectro-temporal projection (Figures 3B and 4B) by integration over all spatial locations (3D × 3D). This projection shows when and at which frequencies a cluster was active irrespective of the spatial location of synchronization.

Further Analyses of Identified Networks

To analyze further properties of a network (modulations in power, other coherence contrasts, and single-trial analysis), we proceeded as follows: To account for interindividual differences, for each subject, we identified the connections within the network that were statistically significant (we computed t-statistics for each connection in the cluster between conditions using STCP; $p < 0.05$, one tailed). We averaged the property of interest (e.g., signal power) across each subject's significant connections and used the resulting values for further analyses and tests. Importantly, the statistical sensitivity of these secondary tests is much higher than for the initial network-identification. The network-identification accounts for a massive multiple-comparison problem, whereas the secondary analyses use only a single test. This explains why the beta network differs between bounce and pass trials, as shown by a secondary analysis, but is not identified in the less sensitive network identification based on the bounce versus pass contrast.

To analyze the synchronization pattern of the beta network (Figures 3C and 3E), we defined seven regions of interest (ROIs) in source space (Table S1). We selected sources that constitute a local maximum in the spatial network pattern and summed the connections between any two ROIs in the network. For each connection between two ROIs, the result was normalized by the maximum across all ROI-pairs, thresholded at 0.1, and visualized as the width of lines connecting the ROIs on the brain surface.

ROC Analysis

We used ROC analysis to test whether coherence within a network predicted the subjects' percept on a single-trial level (Green and Swets, 1966). We computed a predictive index that approximates the probability with which an ideal observer can predict the percept from the coherence on a single trial. For each subject, the predictive index was estimated as the area under the ROC curve for the distributions of single-trial coherence for bounce and pass trials. We tested for significant deviation of the predictive index from chance level (0.5) using a permutation test (10^4 permutations) (Nichols and Holmes, 2002).

Analysis Software

All data analyses were performed in Matlab (MathWorks, Natick, MA) and C with custom software and several open source Matlab-toolboxes: Fieldtrip (http://www.ru.nl/fcdonders/fieldtrip/), SPM2 (http://www.fil.ion.ucl.ac.uk/spm/), and FastICA (http://www.cis.hut.fi/projects/ica/fastica/).

SUPPLEMENTAL INFORMATION

Supplemental Information includes four figures, one table, and Supplemental Experimental Procedures and can be found with this article online at doi:10.1016/j.neuron.2010.12.027.

ACKNOWLEDGMENTS

We thank T.H. Donner, C. Hipp, T.J. Buschman, J. Roy, G.G. Supp, and E.K. Miller for helpful discussions and comments on the manuscript. This work was supported by grants from the European Union (IST-2005-027268, NEST-PATH-043457, and HEALTH-F2-2008-200728), the German Research Foundation (GRK 1247/1 and 1247/2), and the German Federal Ministry of Education and Research (01GW0561, Neuroimage Nord).

Accepted: November 8, 2010
Published: January 26, 2011

REFERENCES

Barcelo, F., Suwazono, S., and Knight, R.T. (2000). Prefrontal modulation of visual processing in humans. Nat. Neurosci. *3*, 399–403.

Barraclough, N.E., Xiao, D., Baker, C.I., Oram, M.W., and Perrett, D.I. (2005). Integration of visual and auditory information by superior temporal sulcus neurons responsive to the sight of actions. J. Cogn. Neurosci. *17*, 377–391.

Bressler, S.L., and Menon, V. (2010). Large-scale brain networks in cognition: Emerging methods and principles. Trends Cogn. Sci. *14*, 277–290.

Bressler, S.L., Coppola, R., and Nakamura, R. (1993). Episodic multiregional cortical coherence at multiple frequencies during visual task performance. Nature *366*, 153–156.

Buschman, T.J., and Miller, E.K. (2007). Top-down versus bottom-up control of attention in the prefrontal and posterior parietal cortices. Science *315*, 1860–1862.

Bushara, K.O., Hanakawa, T., Immisch, I., Toma, K., Kansaku, K., and Hallett, M. (2003). Neural correlates of cross-modal binding. Nat. Neurosci. *6*, 190–195.

Buzsaki, G., and Draguhn, A. (2004). Neuronal oscillations in cortical networks. Science *304*, 1926–1929.

Corbetta, M., and Shulman, G.L. (2002). Control of goal-directed and stimulus-driven attention in the brain. Nat. Rev. Neurosci. *3*, 201–215.

Dahl, C.D., Logothetis, N.K., and Kayser, C. (2009). Spatial organization of multisensory responses in temporal association cortex. J. Neurosci. *29*, 11924–11932.

Donner, T.H., Siegel, M., Oostenveld, R., Fries, P., Bauer, M., and Engel, A.K. (2007). Population activity in the human dorsal pathway predicts the accuracy of visual motion detection. J. Neurophysiol. *98*, 345–359.

Driver, J., and Noesselt, T. (2008). Multisensory interplay reveals crossmodal influences on 'sensory-specific' brain regions, neural responses, and judgments. Neuron *57*, 11–23.

Driver, J., and Spence, C. (2000). Multisensory perception: Beyond modularity and convergence. Curr. Biol. *10*, R731–R735.

Engel, A.K., Fries, P., and Singer, W. (2001). Dynamic predictions: Oscillations and synchrony in top-down processing. Nat. Rev. Neurosci. *2*, 704–716.

Fogassi, L., Gallese, V., Fadiga, L., Luppino, G., Matelli, M., and Rizzolatti, G. (1996). Coding of peripersonal space in inferior premotor cortex (area F4). J. Neurophysiol. *76*, 141–157.

Fries, P. (2005). A mechanism for cognitive dynamics: Neuronal communication through neuronal coherence. Trends Cogn. Sci. *9*, 474–480.

Ghazanfar, A.A., and Schroeder, C.E. (2006). Is neocortex essentially multisensory? Trends Cogn. Sci. *10*, 278–285.

Gray, C.M., and Singer, W. (1989). Stimulus-specific neuronal oscillations in orientation columns of cat visual cortex. Proc. Natl. Acad. Sci. USA *86*, 1698–1702.

Graziano, M.S., Yap, G.S., and Gross, C.G. (1994). Coding of visual space by premotor neurons. Science *266*, 1054–1057.

Graziano, M.S., Reiss, L.A., and Gross, C.G. (1999). A neuronal representation of the location of nearby sounds. Nature *397*, 428–430.

Green, D.M., and Swets, J.A. (1966). Signal Detection Theory and Psychophysics (New York, NY: Wiley).

Gregoriou, G.G., Gotts, S.J., Zhou, H., and Desimone, R. (2009). High-frequency, long-range coupling between prefrontal and visual cortex during attention. Science *324*, 1207–1210.

Gross, J., Kujala, J., Hamalainen, M., Timmermann, L., Schnitzler, A., and Salmelin, R. (2001). Dynamic imaging of coherent sources: Studying neural interactions in the human brain. Proc. Natl. Acad. Sci. USA *98*, 694–699.

Gross, J., Schmitz, F., Schnitzler, I., Kessler, K., Shapiro, K., Hommel, B., and Schnitzler, A. (2004). Modulation of long-range neural synchrony reflects temporal limitations of visual attention in humans. Proc. Natl. Acad. Sci. USA *101*, 13050–13055.

Gruber, T., Muller, M.M., Keil, A., and Elbert, T. (1999). Selective visual-spatial attention alters induced gamma band responses in the human EEG. Clin. Neurophysiol. *110*, 2074–2085.

Hagmann, P., Cammoun, L., Gigandet, X., Meuli, R., Honey, C.J., Wedeen, V.J., and Sporns, O. (2008). Mapping the structural core of human cerebral cortex. PLoS Biol. *6*, e159.

Haider, B., and McCormick, D.A. (2009). Rapid neocortical dynamics: Cellular and network mechanisms. Neuron *62*, 171–189.

Hall, S.D., Holliday, I.E., Hillebrand, A., Singh, K.D., Furlong, P.L., Hadjipapas, A., and Barnes, G.R. (2005). The missing link: Analogous human and primate cortical gamma oscillations. Neuroimage *26*, 13–17.

Henrie, J.A., and Shapley, R. (2005). LFP power spectra in V1 cortex: The graded effect of stimulus contrast. J. Neurophysiol. *94*, 479–490.

Holm, S. (1979). A simple sequentially rejective multiple test procedure. Scand. J. Stat. *6*, 65–70.

Hummel, F., and Gerloff, C. (2005). Larger interregional synchrony is associated with greater behavioral success in a complex sensory integration task in humans. Cereb. Cortex *15*, 670–678.

Hyvarinen, A. (1999). Fast and robust fixed-point algorithms for independent component analysis. IEEE Trans. Neural Netw. *10*, 626–634.

Jarvis, M.R., and Mitra, P.P. (2001). Sampling properties of the spectrum and coherency of sequences of action potentials. Neural Comput. *13*, 717–749.

Jensen, O., Kaiser, J., and Lachaux, J.P. (2007). Human gamma-frequency oscillations associated with attention and memory. Trends Neurosci. *30*, 317–324.

Jung, T.P., Makeig, S., Humphries, C., Lee, T.W., McKeown, M.J., Iragui, V., and Sejnowski, T.J. (2000). Removing electroencephalographic artifacts by blind source separation. Psychophysiology *37*, 163–178.

Kastner, S., and Ungerleider, L.G. (2000). Mechanisms of visual attention in the human cortex. Annu. Rev. Neurosci. *23*, 315–341.

Kayser, C., Petkov, C.I., and Logothetis, N.K. (2008). Visual modulation of neurons in auditory cortex. Cereb. Cortex *18*, 1560–1574.

Keren, A.S., Yuval-Greenberg, S., and Deouell, L.Y. (2010). Saccadic spike potentials in gamma-band EEG: Characterization, detection and suppression. Neuroimage *49*, 2248–2263.

Kopell, N., Ermentrout, G.B., Whittington, M.A., and Traub, R.D. (2000). Gamma rhythms and beta rhythms have different synchronization properties. Proc. Natl. Acad. Sci. USA *97*, 1867–1872.

Kujala, J., Gross, J., and Salmelin, R. (2008). Localization of correlated network activity at the cortical level with MEG. Neuroimage *39*, 1706–1720.

Lachaux, J.P., Rodriguez, E., Martinerie, J., and Varela, F.J. (1999). Measuring phase synchrony in brain signals. Hum. Brain Mapp. *8*, 194–208.

Lakatos, P., Chen, C.M., O'Connell, M.N., Mills, A., and Schroeder, C.E. (2007). Neuronal oscillations and multisensory interaction in primary auditory cortex. Neuron *53*, 279–292.

Lakatos, P., Shah, A.S., Knuth, K.H., Ulbert, I., Karmos, G., and Schroeder, C.E. (2005). An oscillatory hierarchy controlling neuronal excitability and stimulus processing in the auditory cortex. J. Neurophysiol. *94*, 1904–1911.

Lemus, L., Hernandez, A., and Romo, R. (2009). Neural encoding of auditory discrimination in ventral premotor cortex. Proc. Natl. Acad. Sci. USA *106*, 14640–14645.

Leopold, D.A., and Logothetis, N.K. (1999). Multistable phenomena: Changing views in perception. Trends Cogn. Sci. *3*, 254–264.

Leopold, D.A., Murayama, Y., and Logothetis, N.K. (2003). Very slow activity fluctuations in monkey visual cortex: Implications for functional brain imaging. Cereb. Cortex *13*, 422–433.

Lewis, R., and Noppeney, U. (2010). Audiovisual synchrony improves motion discrimination via enhanced connectivity between early visual and auditory areas. J. Neurosci. *30*, 12329–12339.

Lumer, E.D., Friston, K.J., and Rees, G. (1998). Neural correlates of perceptual rivalry in the human brain. Science *280*, 1930–1934.

Maier, J.X., Chandrasekaran, C., and Ghazanfar, A.A. (2008). Integration of bimodal looming signals through neuronal coherence in the temporal lobe. Curr. Biol. *18*, 963–968.

Meredith, M.A., Allman, B.L., Keniston, L.P., and Clemo, H.R. (2009). Auditory influences on non-auditory cortices. Hear. Res. *258*, 64–71.

Mitra, P.P., and Pesaran, B. (1999). Analysis of dynamic brain imaging data. Biophys. J. *76*, 691–708.

Moore, T., Armstrong, K.M., and Fallah, M. (2003). Visuomotor origins of covert spatial attention. Neuron *40*, 671–683.

Nichols, T.E., and Holmes, A.P. (2002). Nonparametric permutation tests for functional neuroimaging: A primer with examples. Hum. Brain Mapp. *15*, 1–25.

Noesselt, T., Rieger, J.W., Schoenfeld, M.A., Kanowski, M., Hinrichs, H., Heinze, H.J., and Driver, J. (2007). Audiovisual temporal correspondence modulates human multisensory superior temporal sulcus plus primary sensory cortices. J. Neurosci. *27*, 11431–11441.

Nunez, P.L., and Srinivasan, R. (2006). Electric Fields of the Brain (New York, NY: Oxford University Press).

Palva, J.M., Monto, S., Kulashekhar, S., and Palva, S. (2010). Neuronal synchrony reveals working memory networks and predicts individual memory capacity. Proc. Natl. Acad. Sci. USA *107*, 7580–7585.

Pesaran, B., Nelson, M.J., and Andersen, R.A. (2008). Free choice activates a decision circuit between frontal and parietal cortex. Nature *453*, 406–409.

Posner, M.I., and Dehaene, S. (1994). Attentional networks. Trends Neurosci. *17*, 75–79.

Rodriguez, E., George, N., Lachaux, J.P., Martinerie, J., Renault, B., and Varela, F.J. (1999). Perception's shadow: Long-distance synchronization of human brain activity. Nature *397*, 430–433.

Roelfsema, P.R., Engel, A.K., König, P., and Singer, W. (1997). Visuomotor integration is associated with zero time-lag synchronization among cortical areas. Nature *385*, 157–161.

Rose, M., and Buchel, C. (2005). Neural coupling binds visual tokens to moving stimuli. J. Neurosci. *25*, 10101–10104.

Saalmann, Y.B., Pigarev, I.N., and Vidyasagar, T.R. (2007). Neural mechanisms of visual attention: How top-down feedback highlights relevant locations. Science *316*, 1612–1615.

Salinas, E., and Sejnowski, T.J. (2001). Correlated neuronal activity and the flow of neural information. Nat. Rev. Neurosci. *2*, 539–550.

Schneider, T.R., Debener, S., Oostenveld, R., and Engel, A.K. (2008). Enhanced EEG gamma-band activity reflects multisensory semantic matching in visual-to-auditory object priming. Neuroimage *42*, 1244–1254.

Schoffelen, J.M., and Gross, J. (2009). Source connectivity analysis with MEG and EEG. Hum. Brain Mapp. *30*, 1857–1865.

Sekuler, R., Sekuler, A.B., and Lau, R. (1997). Sound alters visual motion perception. Nature *385*, 308.

Senkowski, D., Schneider, T.R., Foxe, J.J., and Engel, A.K. (2008). Crossmodal binding through neural coherence: Implications for multisensory processing. Trends Neurosci. *31*, 401–409.

Serences, J.T., and Yantis, S. (2006). Selective visual attention and perceptual coherence. Trends Cogn. Sci. *10*, 38–45.

Siegel, M., and König, P. (2003). A functional gamma-band defined by stimulus-dependent synchronization in area 18 of awake behaving cats. J. Neurosci. *23*, 4251–4260.

Siegel, M., Donner, T.H., Oostenveld, R., Fries, P., and Engel, A.K. (2007). High-frequency activity in human visual cortex is modulated by visual motion strength. Cereb. Cortex *17*, 732–741.

Siegel, M., Donner, T.H., Oostenveld, R., Fries, P., and Engel, A.K. (2008). Neuronal synchronization along the dorsal visual pathway reflects the focus of spatial attention. Neuron *60*, 709–719.

Stein, B.E., and Meredith, M.A. (1993). The Merging of the Senses (Cambridge, MA: The MIT Press).

Sterzer, P., Kleinschmidt, A., and Rees, G. (2009). The neural bases of multistable perception. Trends Cogn. Sci. *13*, 310–318.

Tallon-Baudry, C., Bertrand, O., Delpuech, C., and Pernier, J. (1996). Stimulus specificity of phase-locked and non-phase-locked 40 Hz visual responses in human. J. Neurosci. *16*, 4240–4249.

Thomson, D.J. (1982). Spectrum estimation and harmonic analysis. Proc. IEEE *70*, 1055–1096.

Tootell, R.B., Reppas, J.B., Kwong, K.K., Malach, R., Born, R.T., Brady, T.J., Rosen, B.R., and Belliveau, J.W. (1995). Functional analysis of human MT and related visual cortical areas using magnetic resonance imaging. J. Neurosci. *15*, 3215–3230.

Uhlhaas, P.J., and Singer, W. (2006). Neural synchrony in brain disorders: Relevance for cognitive dysfunctions and pathophysiology. Neuron *52*, 155–168.

Van Veen, B.D., van Drongelen, W., Yuchtman, M., and Suzuki, A. (1997). Localization of brain electrical activity via linearly constrained minimum variance spatial filtering. IEEE Trans. Biomed. Eng. *44*, 867–880.

Varela, F., Lachaux, J.P., Rodriguez, E., and Martinerie, J. (2001). The brainweb: Phase synchronization and large-scale integration. Nat. Rev. Neurosci. *2*, 229–239.

von Stein, A., Chiang, C., and König, P. (2000). Top-down processing mediated by interareal synchronization. Proc. Natl. Acad. Sci. USA *97*, 14748–14753.

Womelsdorf, T., Fries, P., Mitra, P.P., and Desimone, R. (2006). Gamma-band synchronization in visual cortex predicts speed of change detection. Nature *439*, 733–736.

Womelsdorf, T., Schoffelen, J.M., Oostenveld, R., Singer, W., Desimone, R., Engel, A.K., and Fries, P. (2007). Modulation of neuronal interactions through neuronal synchronization. Science *316*, 1609–1612.

Wyart, V., and Tallon-Baudry, C. (2008). Neural dissociation between visual awareness and spatial attention. J. Neurosci. *28*, 2667–2679.

Yuval-Greenberg, S., Tomer, O., Keren, A.S., Nelken, I., and Deouell, L.Y. (2008). Transient induced gamma-band response in EEG as a manifestation of miniature saccades. Neuron *58*, 429–441.